ACS OMEGA

Open Access

This article is licensed under CC-BY-NC-ND 4.0

http://pubs.acs.org/journal/acsodf

Article

Unusual Transport Properties of CNT-Nickelocene-Based Circuits: Role of Structural Symmetry

Jiulin Tang, Hao Wang, Xinghui Tang, Yongjie Zhang, and Chun Zhang*

Cite This: *ACS Omega* 2025, 10, 15250−15255

Read Online

ACCESS | Metrics & More | Article Recommendations | Supporting Information

ABSTRACT: At the nano- or molecular scale, electron transport is often governed by quantum effects, for which the symmetry of the system could become a key factor. In this work, by state-of-the-art first-principles modeling and simulation, we show that the structural symmetry plays a unique role in properties of electronic circuits made of CNT (5,5) electrodes and nickelocene ($NiCp_2$) molecules, resulting in unusual transport phenomena beyond the classical circuit theories. For a single $NiCp_2$ molecule sandwiched between two CNT (5,5) electrodes, we find that the symmetry change caused by the rotation of one CNT electrode greatly affects the conductance of the device, which may have important implications for understanding the performances of CNT-based quantum devices. We further show that when two $NiCp_2$ molecular resistors are connected in series, the conductance of the resulting series-$NiCp_2$ circuit can be significantly higher than the single-$NiCp_2$ device at certain biases, in which the structural symmetry of the circuit plays a critical role. These results provide new opportunities for the future design of molecular devices with novel functions.

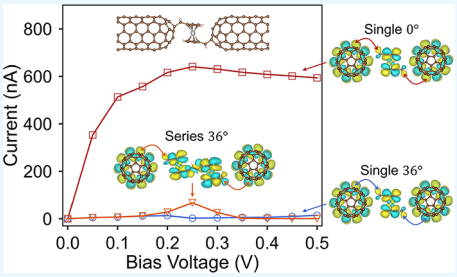

INTRODUCTION

Over the past two decades, an escalating demand for the miniaturization of electronic devices has sparked great interest in the realm of molecular electronics. A great number of single-molecule devices have been proposed to fulfill diverse functionalities, which include single-molecule diodes,[1−3] high-performance molecular transistors,[4−6] light-driven molecular switches,[7−9] and novel spintronic devices.[10−12] Both theoretical and experimental works have shown that the scattering of Bloch electrons from the electrode by the molecular center is the key that determines the transport properties of these devices. The scattering of Bloch electrons can be sensitively dependent on the local molecule-electrode interface,[13−16] and also the structural symmetry of the whole device,[17−21] both of which could lead to intriguing transport properties that can be useful for applications. We are particularly interested in the effects of device symmetry on quantum transport properties, which has become one of the most interesting research directions in molecular electronics. In this work, we show by state-of-the-art first-principles modeling that in molecular devices and circuits made of carbon nanotubes (CNTs) and nickelocene ($NiCp_2$) molecules, the symmetry plays a unique role, which leads to unusual transport phenomena that are beyond classical circuit theories. These findings provide new insights into understanding the performance of CNT-based devices and open new avenues for the future design of novel molecular devices.

Since S. Iijima's pioneering description of CNTs in 1991,[22] CNTs have emerged as materials of significant interest for the next generation of electronic devices.[23−27] It has also been shown that CNTs could be used as optimal electrodes for molecular devices.[28,29] On the other hand, the possibility of building various functional devices with centrosymmetric $NiCp_2$ molecules has been demonstrated both theoretically and experimentally.[30−33] The devices made of CNT electrodes and center $NiCp_2$ molecules could be interesting and realistic platforms to study symmetry effects. In this work, structure optimizations of devices were performed with spin-polarized density functional theory (DFT) using SIESTA.[34] Transport calculations were done with the steady-state density functional theory (SS-DFT)[35,36] that has been proven effective in describing nonequilibrium quantum transport properties of molecular junctions under a finite bias.[37,38] In all calculations, Troullier-Martins pseudopotentials[39] for core electrons and double-ζ polarized (DZP) basis set were employed. The generalized gradient approximation (GGA) of the exchange-correlation functional in the Perdew−Burke−Ernzerhof (PBE)[40] format with nonequilibrium corrections[41,42] is adopted. The convergence criteria for the density matrix, energy, and force in the calculations were set to be 10^{-4}, 10^{-4} eV, and 0.01 eV/Å, respectively.

Received: December 6, 2024
Revised: February 21, 2025
Accepted: March 3, 2025
Published: April 9, 2025

© 2025 The Authors. Published by American Chemical Society

RESULTS AND DISCUSSION

The optimized structure of the single-$NiCp_2$ device is shown in Figure 1a, where two electrodes are capped CNT (5,5), and

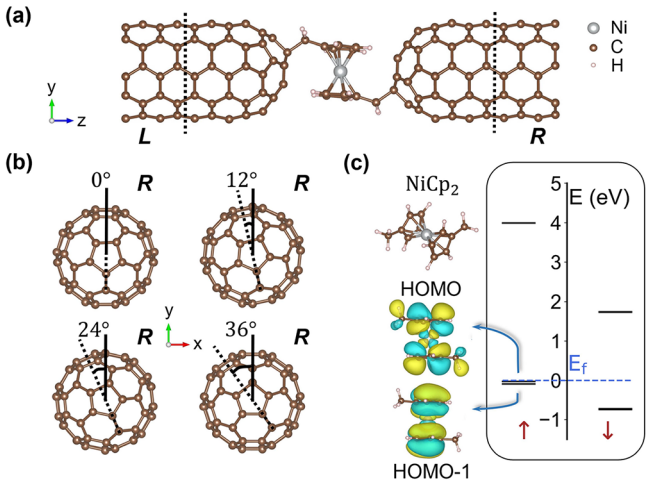

Figure 1. (a) Optimized structure of the CNT-single $NiCp_2$-CNT junction in the centrosymmetric configuration. The $NiCp_2$ molecule is attached to CNTs with CH_2 groups. (b) Right CNT (5,5) electrode with different rotational angles with respect to the z axis. Note that the centrosymmetric structure shown in (a) corresponds to the right electrode with the 0° rotational angle. (c) Energy levels and wave functions of frontier orbitals near the Fermi energy of the $NiCp_2$ molecule with attached CH_3 groups.

the $NiCp_2$ molecule is connected to two CNT electrodes via linker CH_2 groups. It should be noted that the centrosymmetric configuration of the device as shown in the figure is the lowest-energy state among all possible structures we tested, as shown in Figure S1 and Table S1. In structure optimizations, the two outermost unit cells of electrodes (L and R in the figure) are fixed to ground-state structures of infinite CNT (5,5), and the center scattering region is fully relaxed. Starting from this structure, we study the effects of the rotation of the right CNT (5,5) electrode with respect to the z-axis on the electronic and transport properties of the device. The rotational angle is defined as the angle relative to the lowest-energy state, as shown in Figure 1b. Given the 5-fold symmetry of CNT (5,5), we only need to consider the angles ranging from 0 to 36°. For each rotational angle shown in Figure 1b, the device structure is reoptimized. The optimized $NiCp_2$ devices with different rotational angles (0, 12, 24, and 36°) are shown in Figure S1, where we see that the 36°-configuration is mirror-symmetric.

To understand electron transport through the device, we first analyze the electronic structure of the $NiCp_2$ molecule with two CH_3 groups on both ends. The $NiCp_2$ molecule exhibits a total magnetic moment of 2 μ_B, primarily contributed by the 3d orbitals of the nickel atom as shown by the calculated spin density in Figure S2. Additionally, the molecule's energy level diagram (Figure 1c) indicates that the highest occupied molecular orbital (HOMO) and HOMO−1 in the spin-up (majority spin) channel are right below the Fermi energy and almost degenerate with an energy difference of around 0.06 eV. The spin-down (minority spin) orbitals are at least 0.6 eV away from the Fermi energy. As shown by wave function plots in Figure 1c, the spin-up HOMO is extending across the whole molecule, while the HOMO−1 is localized in the middle with zero contributions from two CH_3 groups. This analysis suggests that at low biases the electron transport shall be mainly contributed by tunneling through the spin-up HOMO.

We then calculated spin-dependent current−voltage (I−V) characteristics of the device with different rotational angles for bias voltages from 0 to 0.5 V. Results are shown in Figure 2a.

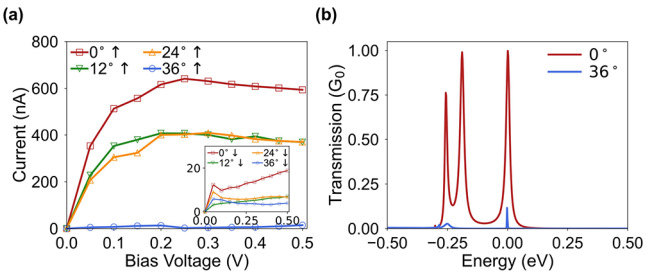

Figure 2. (a) Spin-up I−V curves of single-$NiCp_2$ devices in 0-, 12-, 24-, and 36°-configurations. The inset plots the spin-down I−V curves. (b) Spin-up transmission functions of single-$NiCp_2$ devices for 0- and 36°-configurations at zero bias. The Fermi energy is set to 0 eV.

Except for the 36°-configuration, in all other cases, as expected, the electron transport is dominated by the spin-up channel. For the 36°-configuration, both spin-up and spin-down currents are very low, indicating that both spin channels, in this case, are nonconducting. Surprisingly, from the figure, we see that when the rotational angle of the right CNT electrode changes from 0 to 36°, the electric current at low biases in general drops by at least 1 order of magnitude. As an example, at 0.5 V, the current for the 0°-configuration is about 594 nA, while the current drops to around 14 nA for the 36°-configuration. The huge differences between the transport properties of these two configurations can be confirmed by the calculated transmission functions for two cases under zero bias for the spin-up channel (Figure 2b), where we see that the transmission at the Fermi energy of the 0°-configuration is an order-of-magnitude higher than that of the 36°-configuration. As a reference, the calculated transmissions as functions of energy for all 4 configurations with different rotational angles are plotted in Figures S3 and S4.

To shed light on the order-of-magnitude difference in conductance between 0- and 36°-configurations, we plot the calculated spin-up tunneling eigen channels at Fermi energy for two configurations in Figure 3a. By comparing the eigenchannels in Figure 3a and molecular orbitals in Figure 1c, in both cases, electrons tunnel through spin-up HOMO of the molecule, while it is the different coupling between the $NiCp_2$ HOMO with two CNT electrodes in two cases that causes the huge difference in conductance. For the 0°-configuration, the $NiCp_2$ HOMO couples well with both CNT electrons, leading to a high conductance, while for the 36°-configuration, the $NiCp_2$ HOMO connects well with only one CNT electrode, causing low conductance in this case. The different molecule-electrode couplings for these two configurations can be attributed to different symmetries of these cases, as depicted in Figure 3b. The 0°-configuration device possesses the same symmetry as the molecule, both of which are centrosymmetric. The conducting π orbital of CNT electrodes at Fermi energy and the molecule HOMO in this case are plotted in the upper panel of Figure 3b, where we see

https://doi.org/10.1021/acsomega.4c11037
ACS Omega 2025, 10, 15250−15255

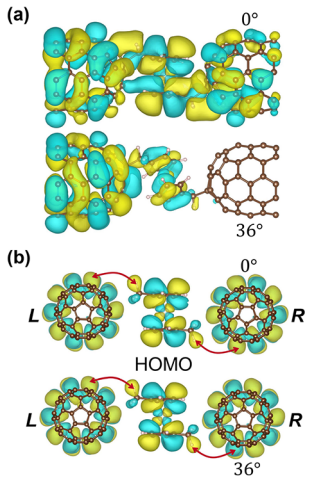

Figure 3. (a) Tunneling eigenchannels of single-$NiCp_2$ devices for 0- and 36°-configurations at zero bias. (b) Schematic models for phase matching between the HOMO of $NiCp_2$ and the conducting π orbital of CNT(5,5) electrodes. Note the in-phase couplings with both electrodes for the 0°-configuration and the out-of-phase coupling with the right electrode for the 36°-configuration.

that the phase of the molecular HOMO matches well with both electrodes, leading to a nice coupling of the molecule with two electrodes. In contrast, the 36°-configuration device possesses the mirror symmetry. By comparing the phases of the molecule and electrode conducting orbitals, we see that the molecule orbital can be in phase with only one electrode, resulting in bad coupling with the other one. It is worth mentioning here that the rotational-angle dependence of the conductance of CNT-based devices is rarely discussed in previous studies. To see if the observed significant rotational-angle dependence of conductance is general for CNT-based devices, we performed transport calculations for a CNT-benzene-CNT junction. The optimized structures and calculated I−V curves for 0- and 36°-configurations are shown in Figure S5. We see a similar trend that the 0°-configuration generates much higher current than the 36°-configuration. This analysis emphasizes the importance of the relative rotation of two CNT electrodes for understanding the transport properties of CNT-based devices.

We next consider a circuit made of two CNT (5,5) electrodes and two $NiCp_2$ molecules connected in series as shown in Figure 4a, which is denoted as a series $NiCp_2$ circuit

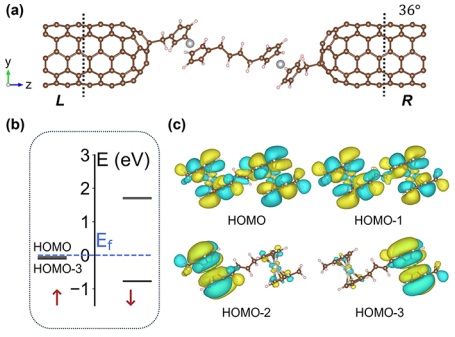

Figure 4. (a) Optimized structure of the series $NiCp_2$ circuit. (b) Energy levels of the series connected two $NiCp_2$ molecules with attached CH_3 groups. (c) Wave function plots for spin-up HOMO, HOMO−1, HOMO−2, and HOMO−3.

in this work. In the circuit, two CNT (5,5) are in mirror symmetry and two $NiCp_2$ molecules are linked by a CH_2−CH═CH−CH_2 functional group that is an often-used metallocene linker in experimental settings.[43,44] The energy levels of the two $NiCp_2$ molecules in series are shown in Figure 4b. Near the Fermi level, four spin-up orbitals, from HOMO to HOMO−3, are nearly degenerate, where only the anticentrosymmetric HOMO and the centrosymmetric HOMO−1 are extended across the two $NiCp_2$ molecules (Figure 4c).

We calculate the spin-dependent I−V curves for the series of $NiCp_2$ junctions. Results are shown in Figure 5a. As a reference, the I−V curves of the single $NiCp_2$ junction with mirror-symmetric CNT (5,5) (the 36°-configuration) are also plotted in the figure. First, we see from the figure that the series $NiCp_2$ circuit is a nearly perfect spin filter that produces spin filtering efficiency (defined as $(I_\uparrow - I_\downarrow)/(I_\uparrow + I_\downarrow)$) higher than 99% at the whole bias range (0 to 0.5 V) under study (see inset of Figure 5a). More importantly, at biases ranging from 0.15 to 0.3 V, the series $NiCp_2$ circuit exhibits significantly higher conductance than the single $NiCp_2$ device, which cannot be explained by classical circuit theories. The spin-up transmission function as a function of energy for the series $NiCp_2$ circuit at 0.25 V is shown in Figure 5b, where we see that in this case, HOMO is the main contributor to the current as only HOMO is inside the bias window. Also, the HOMO presents much higher transmission than the HOMO−1, which can be explained by the different symmetries of two orbitals, as depicted in Figure 5c: The anticentrosymmetric HOMO couples well with the two mirror-symmetric CNT electrodes, while the centrosymmetric HOMO−1 is in phase when coupled with the left electrode but out of phase with the right one. The in-phase coupling of HOMO with both CNT electrodes leads to high conductance when tunneling through HOMO, which is distinctly different from the case of the single $NiCp_2$, where HOMO is out-of-phase with one electrode, resulting in low conductance (Figure 3). To explain the bias dependence of the calculated I−V curve of the series $NiCp_2$ circuit, we plot in Figure 5d the variations of HOMO and HOMO−1 energies with bias voltages obtained from the analysis based on the molecule projected self-consistent Hamiltonian (MPSH), which shows that the HOMO−1 is always outside the bias window; therefore, it does not contribute to the current. In contrast, the HOMO enters the bias window after 0.1 V and starts to exit after the 0.3 V, yielding high conductance of the series circuit at this bias range and the negative differential resistance beyond 0.25 V. It is worth mentioning here that the NDR has been known to be a general phenomenon in transport properties of nanoscale electronic devices.[45−47]

■ CONCLUSIONS

In conclusion, by state-of-the-art first-principles modeling and simulations, we show that the symmetry plays a unique and critical role in quantum electron transport through a circuit made of two CNT (5,5) electrodes and $NiCp_2$ molecules in the middle. For the single-$NiCp_2$ device, we find that the relative rotational angles of two CNT electrodes with respect to the transport axis can dramatically change the conductance of the device due to the different symmetries at different angles. To know the relative rotational angle of CNT electrodes, therefore, can be a key factor in understanding CNT-based quantum devices. For the series-$NiCp_2$ circuit, we predict that at certain bias voltages, the series connection of

https://doi.org/10.1021/acsomega.4c11037
ACS Omega 2025, 10, 15250−15255

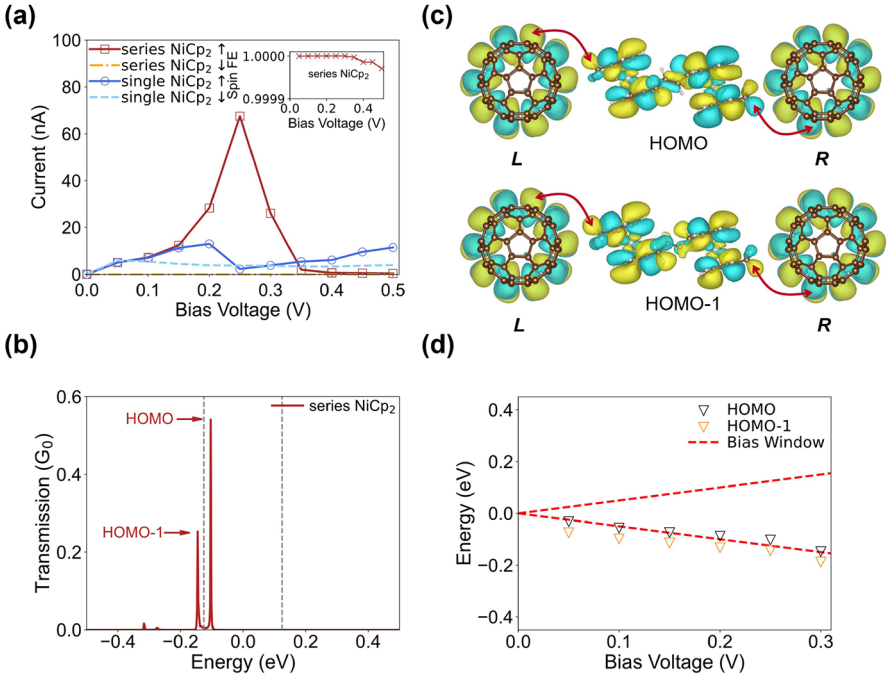

Figure 5. (a) Spin-dependent I−V curves of the single-$NiCp_2$ device and the series $NiCp_2$ circuit in a 36°-configuration. The inset plots the spin-filtering efficiency of the series $NiCp_2$ circuit. (b) Spin-up transmission of the series $NiCp_2$ circuit at 0.25 V. The Fermi energy is set to 0 eV, and two gray dashed lines denote the bias window. (c) Schematic models for phase matching between the conducting π orbital of CNT(5,5) electrodes and two frontier orbitals (HOMO and HOMO−1) of two $NiCp_2$ molecules in series. (d) Variations of front-orbital energies of the series $NiCp_2$ circuit as a function of external bias voltages calculated from MPSH analysis. Red dashed lines indicate the bias window.

two $NiCp_2$ molecules could produce significantly higher conductance than that of single $NiCp_2$ molecule, which is beyond classical circuit theories. The higher conductance of the series circuit can also be attributed to the unique symmetries of conducting frontier orbitals of the series connection of two molecules. We expect this work to stimulate future experimental verifications.

■ ASSOCIATED CONTENT

Supporting Information

The Supporting Information is available free of charge at https://pubs.acs.org/doi/10.1021/acsomega.4c11037.

Optimized structures of single-$NiCp_2$ devices in different configurations, spin densities of $NiCp_2$ molecules, spin-up transmission functions of single-$NiCp_2$ devices, and transport calculations of CNT-benzene-CNT junctions (PDF)

■ AUTHOR INFORMATION

Corresponding Author

Chun Zhang − *Department of Physics, National University of Singapore, Singapore 117551, Singapore; Department of Chemistry, National University of Singapore, Singapore 117543, Singapore;* orcid.org/0000-0002-1581-5806; Email: phyzc@nus.edu.sg

Authors

Jiulin Tang − *Department of Physics, National University of Singapore, Singapore 117551, Singapore*

Hao Wang − *Department of Physics, National University of Singapore, Singapore 117551, Singapore*

Xinghui Tang − *Department of Physics, National University of Singapore, Singapore 117551, Singapore*

Yongjie Zhang − *Department of Physics, National University of Singapore, Singapore 117551, Singapore; Department of Mechanical and Energy Engineering, Southern University of Science and Technology, Shenzhen, Guangdong 518055, China*

Complete contact information is available at: https://pubs.acs.org/10.1021/acsomega.4c11037

Notes

The authors declare no competing financial interest.

■ ACKNOWLEDGMENTS

We acknowledge the support of NUS academic research fund (A-8002944-00-00). The calculations were performed on computational facilities of NUS HPC and the National Supercomputing Centre (NSCC), Singapore.

■ REFERENCES

(1) Aviram, A.; Ratner, M. A. Molecular rectifiers. *Chem. Phys. Lett.* **1974**, *29* (2), 277−283.

(2) Martin, A. S.; Sambles, J. R.; Ashwell, G. J. Molecular rectifier. *Phys. Rev. Lett.* **1993**, *70* (2), 218−221.

(3) Elbing, M.; Ochs, R.; Koentopp, M.; Fischer, M.; von Hänisch, C.; Weigend, F.; Evers, F.; Weber, H. B.; Mayor, M. A single-molecule diode. *Proc. Natl. Acad. Sci. U. S. A.* **2005**, *102* (25), 8815−8820.

(4) Fuechsle, M.; Miwa, J. A.; Mahapatra, S.; Ryu, H.; Lee, S.; Warschkow, O.; Hollenberg, L. C. L.; Klimeck, G.; Simmons, M. Y. A single-atom transistor. *Nat. Nanotechnol.* **2012**, *7* (4), 242−246.

(5) Kubatkin, S.; Danilov, A.; Hjort, M.; Cornil, J.; Brédas, J.-L.; Stuhr-Hansen, N.; Hedegård, P.; Bjørnholm, T. Single-electron transistor of a single organic molecule with access to several redox states. *Nature* **2003**, *425* (6959), 698−701.

(6) Tans, S. J.; Verschueren, A. R. M.; Dekker, C. Room-temperature transistor based on a single carbon nanotube. *Nature* **1998**, *393* (6680), 49−52.
(7) Feringa, B. L.; Van Delden, R. A.; Koumura, N.; Geertsema, E. M. Chiroptical Molecular Switches. *Chem. Rev.* **2000**, *100* (5), 1789−1816.
(8) Dulić, D.; Van Der Molen, S. J.; Kudernac, T.; Jonkman, H. T.; De Jong, J. J. D.; Bowden, T. N.; Van Esch, J.; Feringa, B. L.; Van Wees, B. J. One-Way Optoelectronic Switching of Photochromic Molecules on Gold. *Phys. Rev. Lett.* **2003**, *91* (20), No. 207402.
(9) Jia, C.; Migliore, A.; Xin, N.; Huang, S.; Wang, J.; Yang, Q.; Wang, S.; Chen, H.; Wang, D.; Feng, B.; et al. Covalently bonded single-molecule junctions with stable and reversible photoswitched conductivity. *Science* **2016**, *352* (6292), 1443−1445.
(10) Moodera, J. S.; Santos, T. S.; Nagahama, T. The phenomena of spin-filter tunnelling. *J. Phys.: Condens. Matter* **2007**, *19* (16), No. 165202.
(11) Bogani, L.; Wernsdorfer, W. Molecular spintronics using single-molecule magnets. *Nat. Mater.* **2008**, *7* (3), 179−186.
(12) Pal, A. N.; Li, D.; Sarkar, S.; Chakrabarti, S.; Vilan, A.; Kronik, L.; Smogunov, A.; Tal, O. Nonmagnetic single-molecule spin-filter based on quantum interference. *Nat. Commun.* **2019**, *10* (1), 5565.
(13) Sen, A.; Kaun, C.-C. Effect of Electrode Orientations on Charge Transport in Alkanedithiol Single-Molecule Junctions. *ACS Nano* **2010**, *4* (11), 6404−6408.
(14) Qian, Z.; Hou, S.; Ning, J.; Li, R.; Shen, Z.; Zhao, X.; Xue, Z. First-principles calculation on the conductance of a single 1,4-diisocyanatobenzene molecule with single-walled carbon nanotubes as the electrodes. *J. Chem. Phys.* **2007**, *126* (8), No. 084705.
(15) Engelkes, V. B.; Beebe, J. M.; Frisbie, C. D. Length-Dependent Transport in Molecular Junctions Based on SAMs of Alkanethiols and Alkanedithiols: Effect of Metal Work Function and Applied Bias on Tunneling Efficiency and Contact Resistance. *J. Am. Chem. Soc.* **2004**, *126* (43), 14287−14296.
(16) Yaliraki, S. N.; Ratner, M. A. Molecule-interface coupling effects on electronic transport in molecular wires. *J. Chem. Phys.* **1998**, *109* (12), 5036−5043.
(17) Li, D.; Banerjee, R.; Mondal, S.; Maliyov, I.; Romanova, M.; Dappe, Y. J.; Smogunov, A. Symmetry aspects of spin filtering in molecular junctions: Hybridization and quantum interference effects. *Phys. Rev. B* **2019**, *99* (11), No. 115403.
(18) Gehring, P.; Thijssen, J. M.; Van Der Zant, H. S. J. Single-molecule quantum-transport phenomena in break junctions. *Nature Reviews Physics* **2019**, *1* (6), 381−396.
(19) Kim, Y.; Song, H.; Strigl, F.; Pernau, H. F.; Lee, T.; Scheer, E. Conductance and vibrational states of single-molecule junctions controlled by mechanical stretching and material variation. *Phys. Rev. Lett.* **2011**, *106* (19), No. 196804.
(20) Venkataraman, L.; Klare, J. E.; Nuckolls, C.; Hybertsen, M. S.; Steigerwald, M. L. Dependence of single-molecule junction conductance on molecular conformation. *Nature* **2006**, *442* (7105), 904−907.
(21) Lawson, J. W.; Bauschlicher, C. W. Transport in molecular junctions with different metallic contacts. *Phys. Rev. B* **2006**, *74* (12), No. 125401.
(22) Iijima, S. Helical microtubules of graphitic carbon. *Nature* **1991**, *354* (6348), 56−58.
(23) Franklin, A. D.; Luisier, M.; Han, S. J.; Tulevski, G.; Breslin, C. M.; Gignac, L.; Lundstrom, M. S.; Haensch, W. Sub-10 nm carbon nanotube transistor. *Nano Lett.* **2012**, *12* (2), 758−762.
(24) Matsuda, Y.; Tahir-Kheli, J.; Goddard, W. A. Definitive Band Gaps for Single-Wall Carbon Nanotubes. *J. Phys. Chem. Lett.* **2010**, *1* (19), 2946−2950.
(25) Avouris, P.; Chen, Z.; Perebeinos, V. Carbon-based electronics. *Nat. Nanotechnol.* **2007**, *2* (10), 605−615.
(26) Chen, Z.; Appenzeller, J.; Knoch, J.; Lin, Y. M.; Avouris, P. The role of metal-nanotube contact in the performance of carbon nanotube field-effect transistors. *Nano Lett.* **2005**, *5* (7), 1497−1502.
(27) Martel, R.; Schmidt, T.; Shea, H. R.; Hertel, T.; Avouris, P. Single- and multi-wall carbon nanotube field-effect transistors. *Appl. Phys. Lett.* **1998**, *73* (17), 2447−2449.
(28) Li, H. J.; Lu, W. G.; Li, J. J.; Bai, X. D.; Gu, C. Z. Multichannel ballistic transport in multiwall carbon nanotubes. *Phys. Rev. Lett.* **2005**, *95* (8), No. 086601.
(29) Guo, X.; Small, J. P.; Klare, J. E.; Wang, Y.; Purewal, M. S.; Tam, I. W.; Hong, B. H.; Caldwell, R.; Huang, L.; O'Brien, S.; et al. Covalently bridging gaps in single-walled carbon nanotubes with conducting molecules. *Science* **2006**, *311* (5759), 356−359.
(30) Mohr, M.; Gruber, M.; Weismann, A.; Jacob, D.; Abufager, P.; Lorente, N.; Berndt, R. Spin dependent transmission of nickelocene-Cu contacts probed with shot noise. *Phys. Rev. B* **2020**, *101* (7), No. 075414.
(31) Ormaza, M.; Abufager, P.; Verlhac, B.; Bachellier, N.; Bocquet, M. L.; Lorente, N.; Limot, L. Controlled spin switching in a metallocene molecular junction. *Nat. Commun.* **2017**, *8* (1), 1974.
(32) Bachellier, N.; Ormaza, M.; Faraggi, M.; Verlhac, B.; Vérot, M.; Le Bahers, T.; Bocquet, M. L.; Limot, L. Unveiling nickelocene bonding to a noble metal surface. *Phys. Rev. B* **2016**, *93* (19), No. 195403.
(33) Yi, Z.; Shen, X.; Sun, L.; Shen, Z.; Hou, S.; Sanvito, S. Tuning the Magneto-Transport Properties of Nickel−Cyclopentadienyl Multidecker Clusters by Molecule−Electrode Coupling Manipulation. *ACS Nano* **2010**, *4* (4), 2274−2282.
(34) Artacho, E.; Anglada, E.; Diéguez, O.; Gale, J. D.; García, A.; Junquera, J.; Martin, R. M.; Ordejón, P.; Pruneda, J. M.; Sánchez-Portal, D.; et al. The SIESTA method; developments and applicability. *J. Phys.: Condens. Matter* **2008**, *20* (6), No. 064208.
(35) Liu, S.; Xi, Y.; Guo, N.; Yam, K. M.; Zhang, C. Spin-dependent electron transport through a Mn-phthalocyanine molecule — A steady-state density functional theory (SS-DFT) study. *Can. J. Chem.* **2016**, *94* (12), 1002−1005.
(36) Liu, S.; Nurbawono, A.; Zhang, C. Density Functional Theory for Steady-State Nonequilibrium Molecular Junctions. *Sci. Rep.* **2015**, *5* (1), 15386.
(37) Wang, H.; Yam, K.-M.; Jiang, Z.; Guo, N.; Zhang, C. Structure phase change induced by nonequilibrium effects in molecular-scale junctions. *Phys. Rev. B* **2024**, *110* (12), L121405.
(38) Jiang, Z.; Yam, K.-M.; Guo, N.; Zhang, L.; Shen, L.; Zhang, C. Prominent nonequilibrium effects beyond the standard first-principles approach in nanoscale electronic devices. *Nanoscale Horizons* **2021**, *6* (10), 801−808.
(39) Troullier, N.; Martins, J. L. Efficient pseudopotentials for plane-wave calculations. *Phys. Rev. B Condens. Matter* **1991**, *43* (3), 1993−2006.
(40) Perdew, J. P.; Burke, K.; Ernzerhof, M. Generalized Gradient Approximation Made Simple. *Phys. Rev. Lett.* **1996**, *77* (18), 3865−3868.
(41) Zhang, C. Uniform electron gas under an external bias: The generalized Thomas-Fermi−Dirac model and the dual-mean-field theory. *J. At. Mol. Sci.* **2014**, *5* (2), 95−99.
(42) Liu, S.; Feng, Y. P.; Zhang, C. Communication: Electronic and transport properties of molecular junctions under a finite bias: A dual mean field approach. *J. Chem. Phys.* **2013**, *139* (19), 191103.
(43) Bunting, H. E.; Green, M. L. H.; Marder, S. R.; Thompson, M. E.; Bloor, D.; Kolinsky, P. V.; Jones, R. J. The synthesis of ferrocenyl compounds with second-order optical non-linearities. *Polyhedron* **1992**, *11* (12), 1489−1499.
(44) Vorotyntsev, M. A.; Vasilyeva, S. V. Metallocene-containing conjugated polymers. *Adv. Colloid Interface Sci.* **2008**, *139* (1), 97−149.
(45) Zhang, C.; et al. Coherent Electron Transport through an Azobenzene Molecule: A Light-Driven Molecular Switch. *Phys. Rev. Lett.* **2004**, *92*, No. 158301.
(46) Cai, Y.; Zhang, A.; Ping Feng, Y.; Zhang, C. Switching and rectification of a single light-sensitive diarylethene molecule sandwiched between graphene nanoribbons. *J. Chem. Phys.* **2011**, *135*, 184703.

https://doi.org/10.1021/acsomega.4c11037
ACS Omega 2025, 10, 15250−15255

(47) Naskar, S.; Das, M. First principle investigations on transport properties in porphyrin, hexaphyrin, and hexathia[26π]annulene molecular junction devices. *Appl. Phys. Lett.* **2020**, *116* (26), 263301.

https://doi.org/10.1021/acsomega.4c11037
ACS Omega 2025, 10, 15250−15255